Preliminary oxidation-assisted derivation strategy from biomass to N, O co-doped carbon used for multifunctional capacitor applications

Xu Zhang[a], Ruichen Zhai[a], Xingchen Jin[a], Shi He[b], Hongmei Li[c*], Ying Chen[a], Lijuan Wei[a], Xutong Yang[a], Shaojie Li[a], YuLan Meng[a], Jiongjiong Mao[c] and Lu Song[d*]*

[a] State Key Laboratory of Fine Chemicals, School of Chemical Engineering, Ocean and Life Sciences, Dalian University of Technology, Panjin 124221, China.

[b] Leicester International Institute, Dalian University of Technology, Panjin 124221, China.

[c] College of Material Science and Engineering, Shenyang Aerospace University (SAU), Shenyang, China.

[d] Department of Materials Science and Engineering, Korea Advanced Institute of Science and Technology (KAIST), 291 Dehak-ro, Yuseong-gu, Daejeon 34141, Republic of Korea.

*Corresponding Author

E-mail addresses: zhangxu@dlut.edu.cn; hmli@sau.edu.cn; songlu@alumni.kaist.ac.kr

1. Materials characterization

Field emission scanning electron microscopy (FE-SEM) and energy dispersive spectroscopy (EDS) were observed by FEI NOVA NanoSEM 450 system. Transmission electron microscopy (TEM) and selected area electron diffraction (SAED) were carried out on FEI Tecnai G2 F30 system. Raman measurements were carried out on Renishaw inVia Raman Microscope using laser excitation at 532 nm. Specific surface area and pore size distribution were calculated according to the data recorded on Quantachrome Autosorb-iQ-C. The data of X-ray photoelectron spectroscopy (XPS) were collected on Thermo ESCALAB 250 photoelectron spectrometer. X-ray diffraction (XRD) patterns were obtained using a Shimadzu XRD-7000S diffractometer with Cu Ka radiation.

2. Electrochemical measurements

The electrochemical properties of the samples were evaluated by the CHI 760E electrochemistry workstation in 6 M KOH solution. The as-prepared samples, carbon black, and binder poly (tetrafluoroethylene) with the mass ratio of 80:10:10 were mixed together by adding a small amount of ethanol, followed by ultrasonic treatment and evaporation of solvent. Then the mixture was rolled into carbon film, which was further dried at 80℃ overnight to obtain the carbon-based electrode. For three electrode tests, the as-obtained samples were used as the working electrode, platinum foil was used as the counter electrode, and Hg/HgO electrode was used as the reference electrode, respectively. For two electrode tests, two work electrodes were symmetrically assembled with a cellulose-based non-woven fabric as separator. The gravimetric

capacitance for a single electrode C_m (F g^{-1}) was calculated according to galvanostatic charge-discharge profiles. For the three-electrode test

$$C_m = \frac{I\Delta t}{m\Delta V}$$

and for the two-electrode test

$$C_m = \frac{2I\Delta t}{m\Delta V}$$

Where C_m is the specific capacitance (F g^{-1}), I is the discharging current (A), Δt is the discharge time (s), m is the mass of active material in a single electrode (g), and ΔV is the potential change during the discharge process, respectively.

For the preparation of zinc-ion hybrid capacitors (ZHCs), different proportions of biomass-derived activated carbon, Super P carbon, aqueous binders (La133 and polyacrylic acid), and carbon nanotubes were thoroughly mixed in a 7:2:0.9:0.1 ratio. The resulting slurry was then coated onto graphite foil, with the active material mass controlled at approximately 1.0 mg cm^{-2}. The slurry was dried at 60℃ for 12 h. The coin cells were assembled in an air atmosphere using 3 M $ZnSO_4$ as the aqueous electrolyte and zinc foil as the negative electrode. The battery performance was tested using a LAND (CT 3002 A) battery testing system.

Energy density (Wh kg^{-1}) and power density (W kg^{-1}) of the electrodes were calculated based on the following equations:

$$E = \frac{1}{2}\frac{C_m}{4}V^2\frac{1}{3.6}$$

$$P = \frac{E}{t}$$

3. Figures

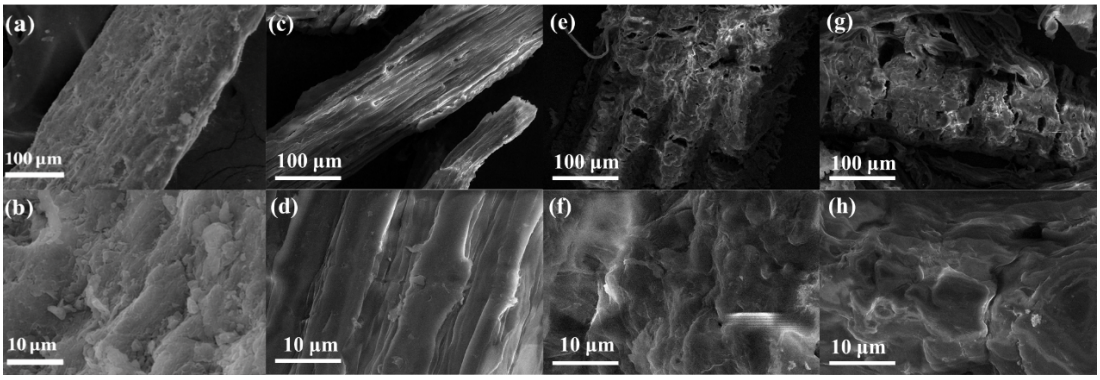

Fig. S1. The SEM images of the rice straw are as follows: (a-b) rice straw, (c-d) NaOH-treated rice straw, (e-f) rice straw treated with NaOH and 10% H_2O_2, and (g-h) rice straw treated with NaOH and 20% H_2O_2.

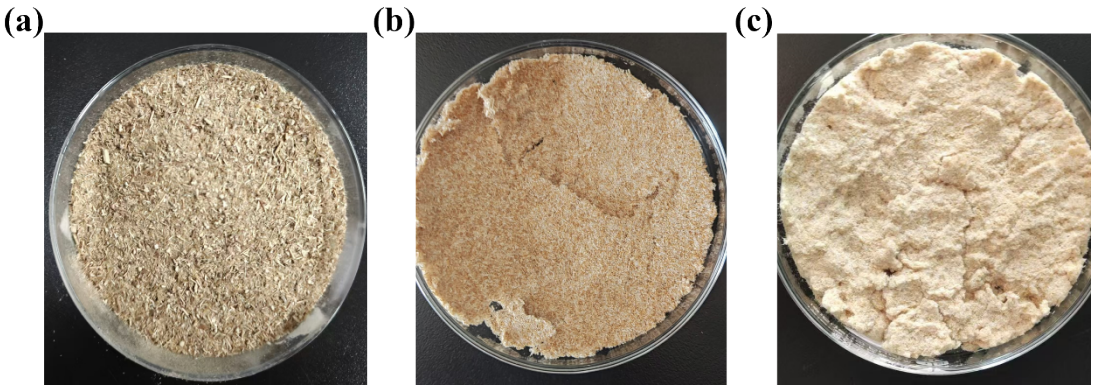

Fig. S2. The digital photos of the rice straw: (a) rice straw precursor, (b) rice straw treated with NaOH, (c) and rice straw treated with NaOH and H_2O_2.

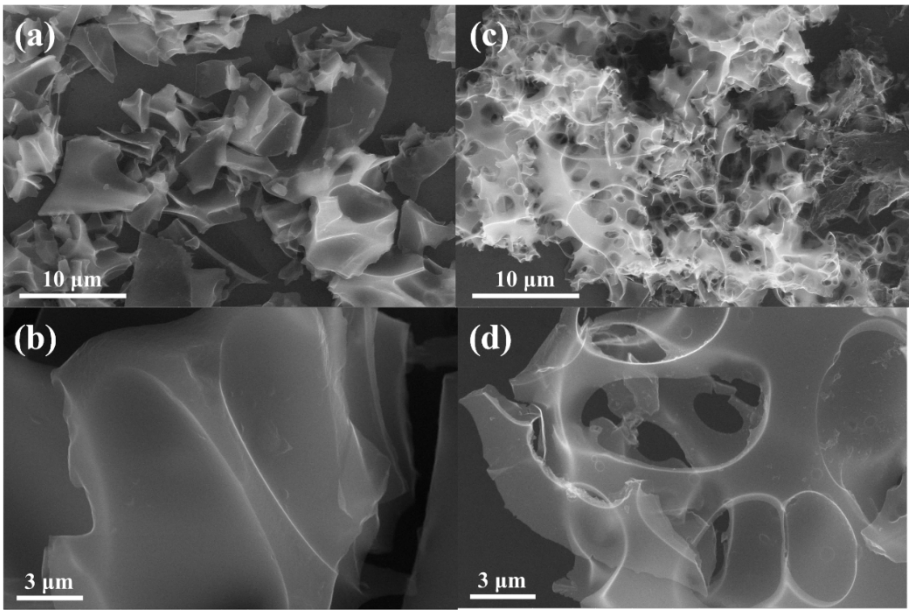

Fig. S3. The SEM images of N-RSC-1:2:5 and N-RSC-1:4:5.

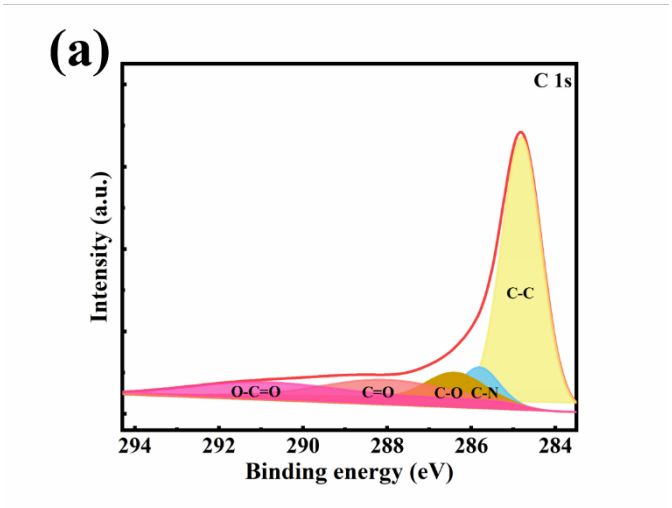

Fig. S4. High resolution XPS spectra of N, O-RSC-10: (a) C 1s.

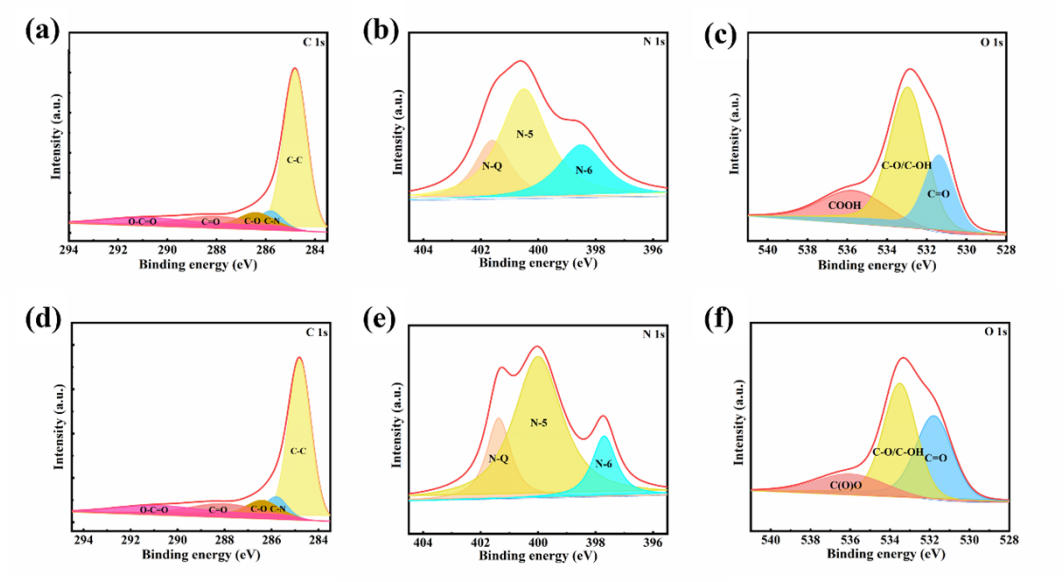

Fig. S5. High resolution XPS spectra namely (a,d) C 1s, (b,e) N 1s, and (c,f) O 1s spectra for N, O-RSC and N, O-RSC-20.

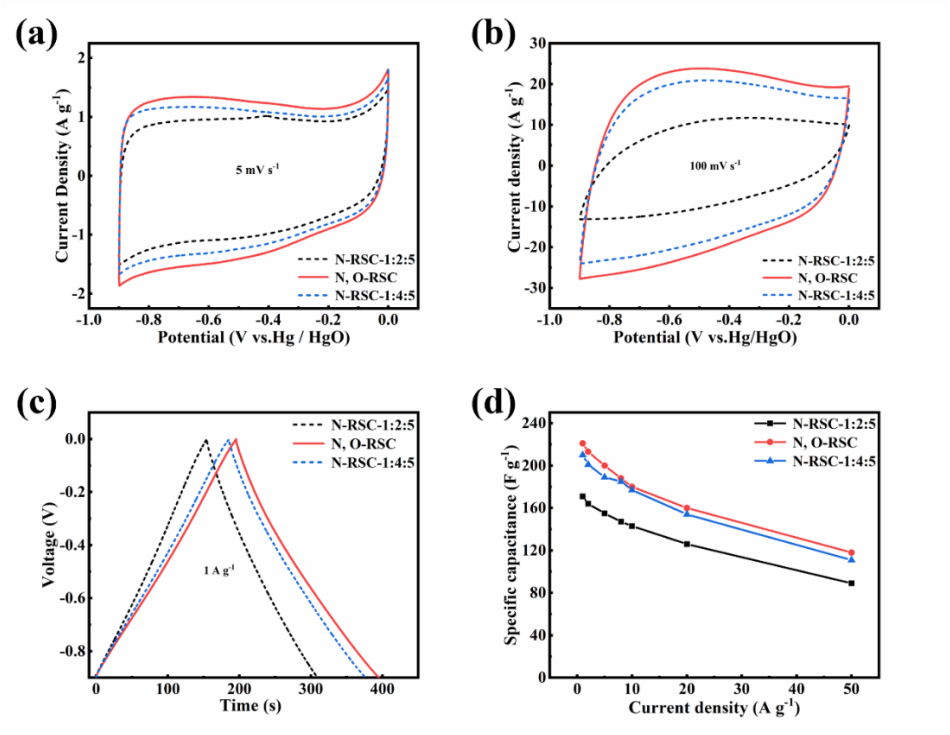

Fig. S6. Cyclic voltammograms of N-RSC-1:2:5, N, O-RSC and N-RSC-1:4:5 at scan rates of (a) 5 mV s^{-1} and (b) 100 mV s^{-1}; (c) galvanostatic charge–discharge curves of N-RSC-1:2:5, N, O-RSC and N-RSC-1:4:5 at a current density of 1 A g^{-1}; (d) specific capacitances of N-RSC-1:2:5, N, O-RSC and N-RSC-1:4:5 at different current densities.

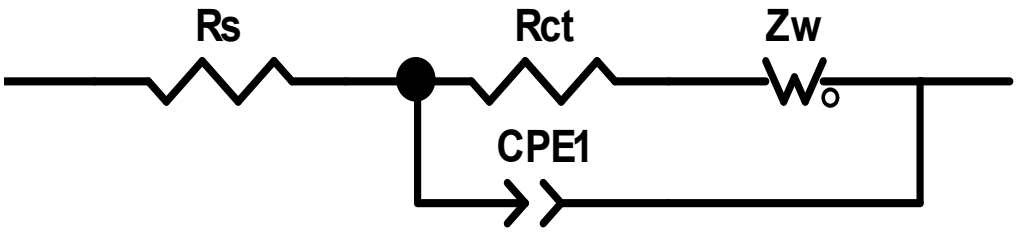

Fig. S7. Equivalent circuit diagram.

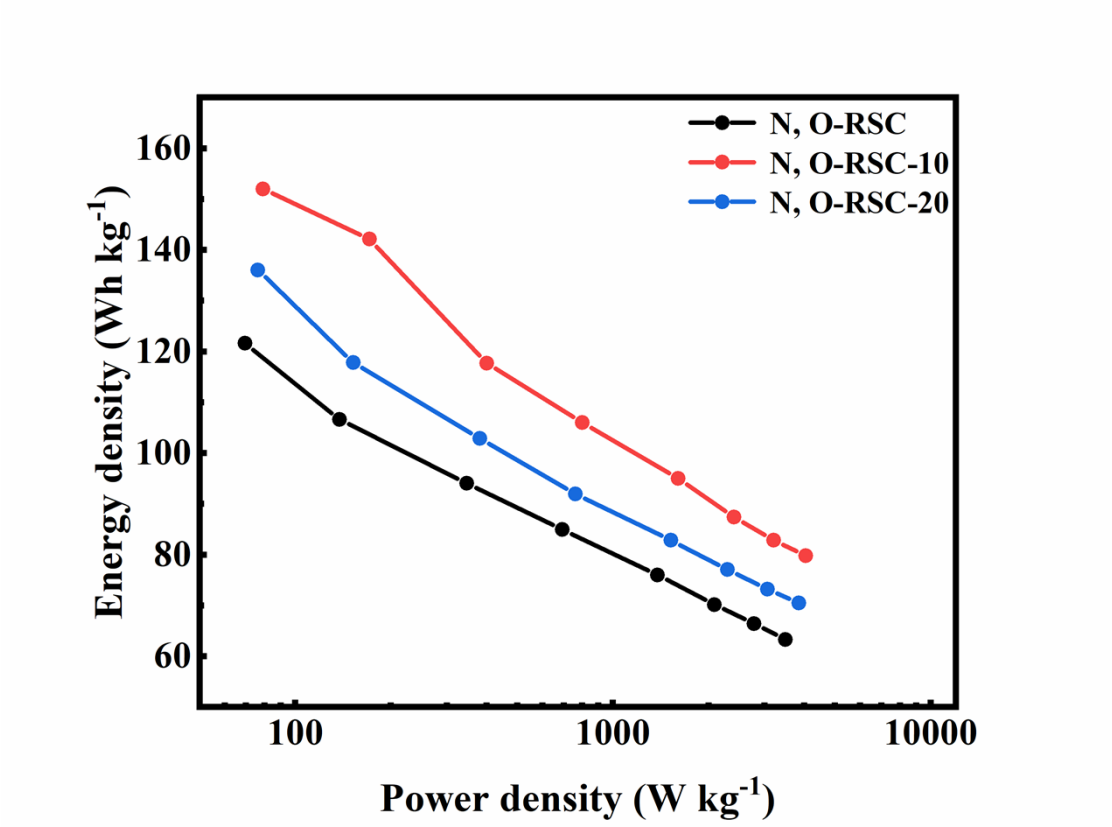

Fig. S8. Ragone plots of N, O-RSCs zinc-ion hybrid supercapacitor.

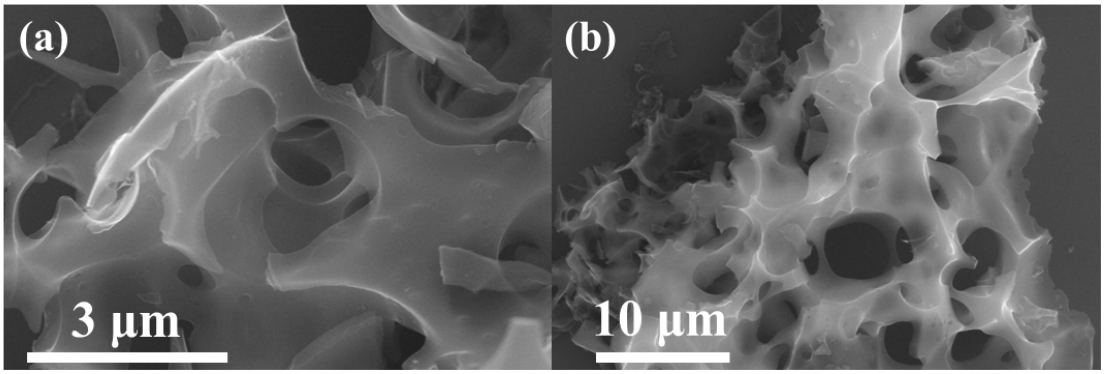

Fig. S9. The SEM images of O-RSC-10.

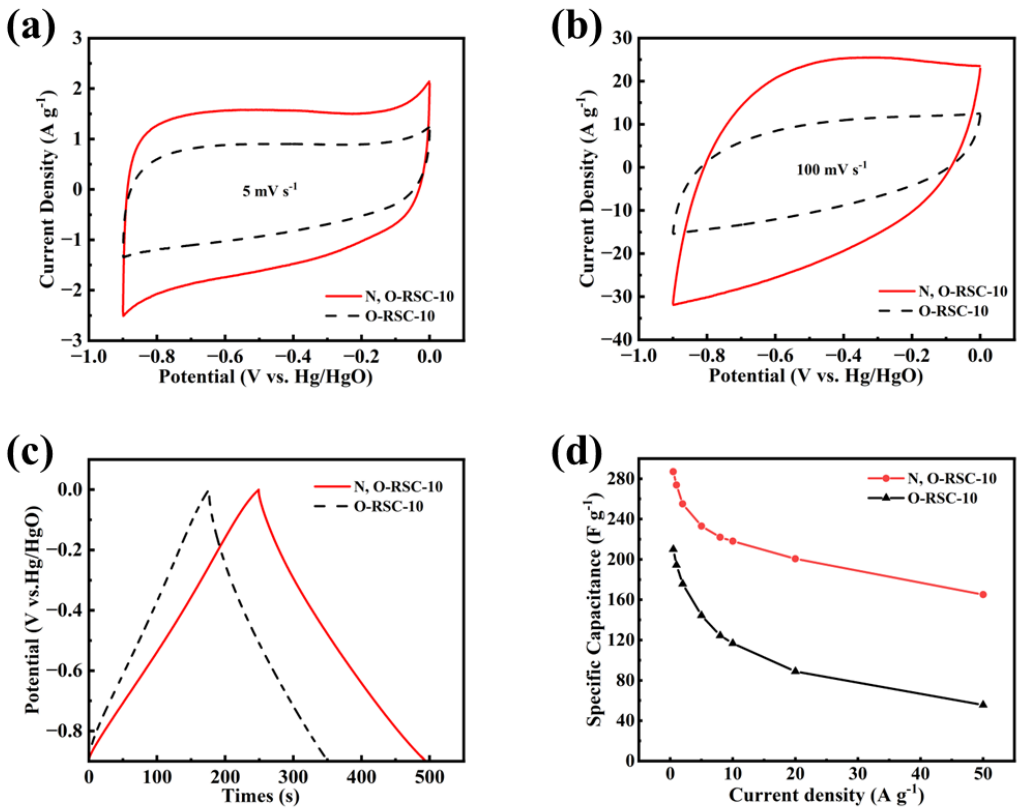

Fig. S10. Cyclic voltammograms of N, O-RSC-10 and O-RSC-10 at scan rates of (a) 5 mV s^{-1} and (b) 100 mV s^{-1}; (c) galvanostatic charge–discharge curves of N, O-RSC-10 and O-RSC-10 at a current density of 1 A g^{-1}; (d) specific capacitances of N, O-RSC-10 and O-RSC-10 at different current densities.

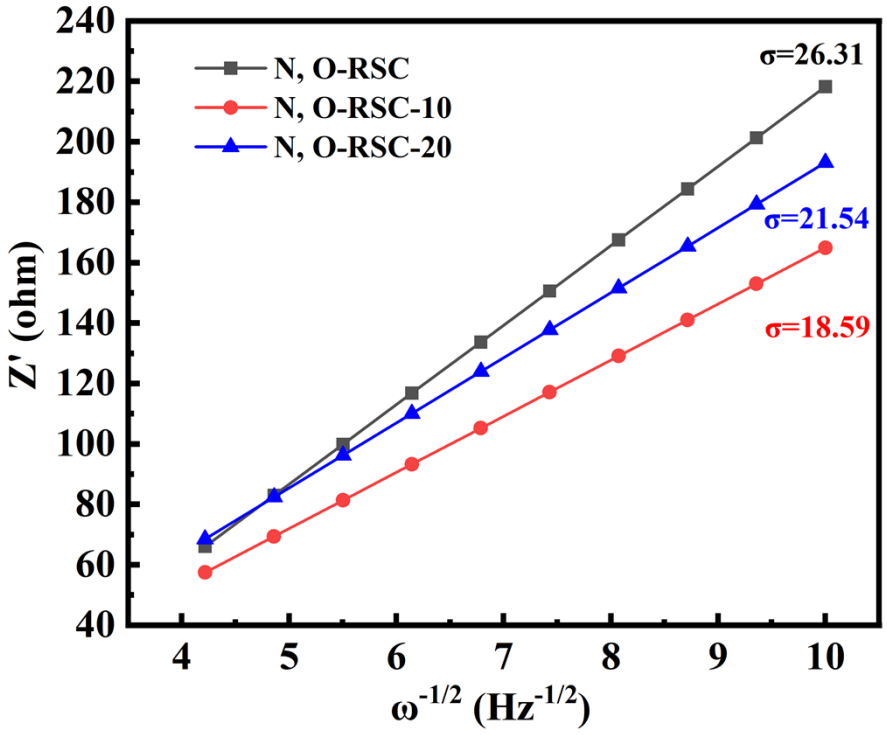

Fig. S11. Z′ vs. $\omega^{-1/2}$ plots.

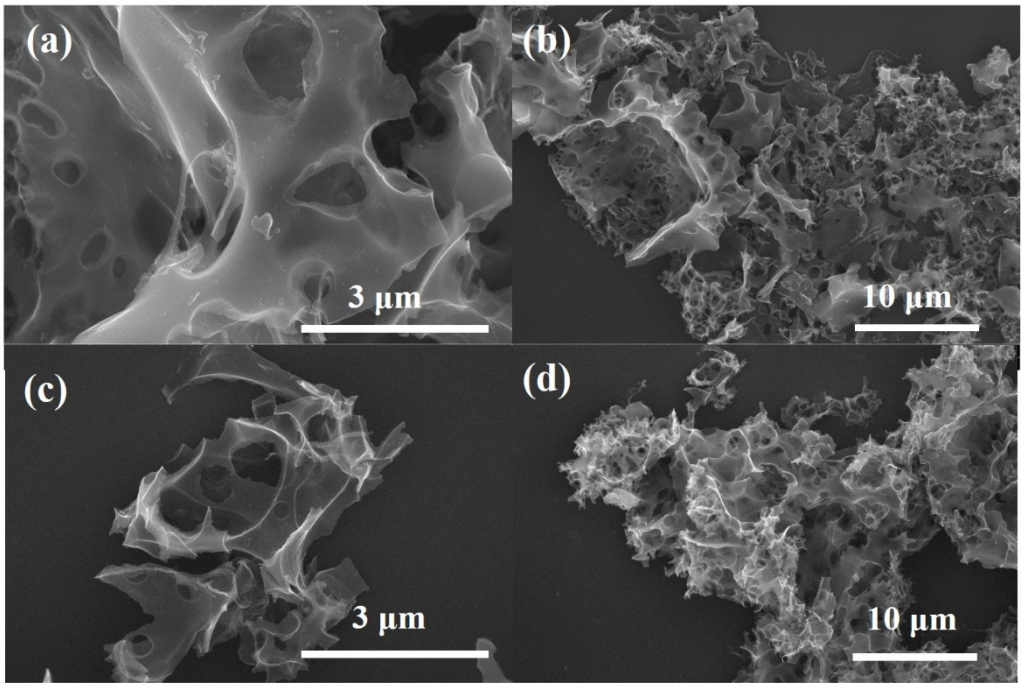

Fig. S12. The SEM images of N, O-RSC-10-600 (a, b) and N, O-RSC-10-800(c, d).

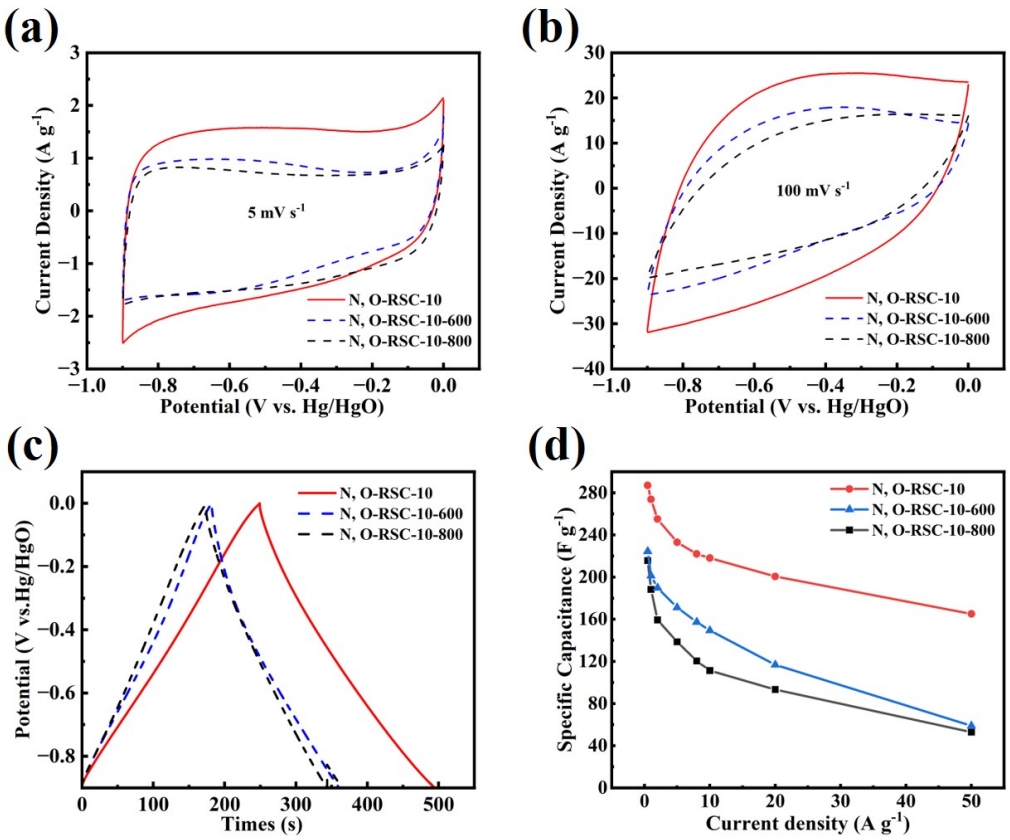

Fig. S13. Cyclic voltammograms of N, O-RSC-10, N, O-RSC-10-600 and N, O-RSC-10-800 at scan rates of (a) 5 mV s^{-1} and (b) 100 mV s^{-1}; (c) galvanostatic charge–discharge curves of N, O-RSC-10, N, O-RSC-10-600 and N, O-RSC-10-800 at a current density of 1 A g^{-1}; (d) specific capacitances of N, O-RSC-10, N, O-RSC-10-600 and N, O-RSC-10-800 at different current densities.

Table S1. Pore structure parameters of N, O-RSCs

Sample	S_{BET} (m^2 g^{-1})	S_{mic} (m^2 g^{-1})	S_{mes} (m^2 g^{-1})	V_{Total} (cm^3 g^{-1})	V_{mic} (cm^3 g^{-1})	Pore size (nm)
N, O-RSC	1661	1125	536	0.95	0.48	2.20
N, O-RSC-10	2103	1842	260	1.16	0.78	1.98
N, O-RSC-20	1718	1161	556	0.92	0.50	2.15

S_{BET}: specific Brunauer-Emmett-Teller surface area;

S_{mic}: micropore surface area;

S_{meso}: mesopore surface area;

V_t: total pore volume;

V_{mic}: micropore volume;

V_{meso}: mesopore volume

Table S2. The content of N, O and C of N, O-RSCs

Sample	C (at%)	N (at%)	O (at%)	H (at%)
N, O-RSC	90.12	1.32	7.78	0.78
N, O-RSC-10	86.35	1.40	11.85	0.40
N, O-RSC-20	81.38	1.47	15.90	1.25

Table S3. Equivalent circuit impedance fitting parameters of all samples

Sample	R_s (Ω)	R_{ct} (Ω)	Z_w (Ω)
N, O-RSC	0.51	3.63	0.62
N, O-RSC-10	0.56	2.58	0.48
N, O-RSC-20	0.59	2.70	0.48

Table S4. Comparison of the specific capacitance of recently reported carbon materials derived from natural biomasses for supercapacitors in aqueous electrolyte.

Materials	Electrolyte	Capacitance (F g^{-1})	Cyclic stability	Cycle number	Ref.
N, O-RSC-10	6 M KOH	273.8 (1 A g^{-1})	93.9%	15000 (10 A g^{-1})	This work
N–S-FHCF (MB)	6 M KOH	235 (1 A g^{-1})	83.4%	3000 (1 A g^{-1})	[S1]
HPCMgK-600	6 M KOH	225.3 (1 A g^{-1})	88%	10000 (5 A g^{-1})	[S2]
BHPC-3	6 M KOH	226.2 (0.5 A g^{-1})	78.4%	5000 (1 A g^{-1})	[S3]
APG-1%	6 M KOH	158.5 (1 A g^{-1})	75.6%	4000 (5 A g^{-1})	[S4]
HHCSs-700	6 M KOH	241 (0.5 A g^{-1})	87.9%	10000 (10 A g^{-1})	[S5]
LUDC_0.5	6 M KOH	177.5 (0.5 A g^{-1})	96%	12000 (10 A g^{-1})	[S6]
N/S-UCN_{600}	6 M KOH	225 (2 A g^{-1})	90.8%	10000 (2 A g^{-1})	[S7]
SC-CSC-7	6 M KOH	105.4 (0.1 A g^{-1})	93.5%	2000 (1 A g^{-1})	[S8]
PC4	6 M KOH	128 (0.5 A g^{-1})	97.3%	2000 (10 A g^{-1})	[S9]
SPAC	1 M H_2SO_4	208.95 (0.06 A g^{-1})	89.7%	1000 (0.08 A g^{-1})	[S10]
LPRAC-20%	6 M KOH	217.3 (0.5 A g^{-1})	95.3%	5000 (20 A g^{-1})	[S11]
LK-800	3 M KOH	255.2 (1 A g^{-1})	99.5%	10000 (10 A g^{-1})	[S12]
PC-Ni/ MnO_2	6 M KOH	267.3 (0.1 A g^{-1})	83.6%	5000 (1 A g^{-1})	[S13]

[S1] J. Lei, Q. Guo, W. Yao, T. Duan, P. Chen and W. Zhu, J. Mater. Chem. A, 2018, 6, 10710-10717.
[S2] K. Chen, S. Weng, J. Lu, J. Gu, G. Chen, O. Hu, X. Jiang and L. Hou, Microporous Mesoporous Mater., 2021, 320, 111106.
[S3] G. Gou, F. Huang, M. Jiang, J. Li and Z. Zhou, Renew. Energy, 2020, 149, 208-216.
[S4] Y. Wang, H. Wang, T. C. Zhang, S. Yuan and B. Liang, J. Power Sources, 2020, 472, 228610.
[S5] H. Liu, M. Han, J. Zuo, X. Deng, W. Lu, Y. Wu, H. Song, C. Zhou and S. Ji, RSC Adv, 2019, 9, 15868-15873.
[S6] L. Chen, J. Deng, Y. Song, S. Hong and H. Lian, Mater. Res. Bull., 2020, 123, 110708.
[S7] L. Miao, H. Duan, M. Liu, W. Lu, D. Zhu, T. Chen, L. Li and L. Gan, Chem. Eng. J., 2017, 317, 651-659.
[S8] L. Cheng, P. Guo, R. Wang, L. Ming, F. Leng, H. Li and X. S. Zhao, Colloids Surf. A, 2014, 446, 127-133.
[S9] S. Guo, B. Guo, R. Ma, Y. Zhu and J. Wang, RSC Adv, 2020, 10, 15707-15714.
[S10] A. Levent and C. Saka, Biomass Convers. Biorefin., 2025, 15, 20803-20816.
[S11] W. Li, G. Wang, W. Sui, T. Xu, Z. Li, A. M. Parvez and C. Si, Carbon, 2022, 196, 819-827.
[S12] S. Gao, H. You, T. Lyu, Y. Gao, M. Chang and F. Wang, Biomass Convers. Biorefin., 2026, 16, 45.
[S13] X. Ji, D. Sun, W. Zou, Z. Wang and D. Sun, J. Alloys Compd., 2021, 876, 160112.